FERMILAB=PUB-20-077-ND-SCD

Probing Nuclear Effects with Neutrino-induced Charged-Current Neutral Pion Production

D. Coplowe,[1] O. Altinok,[2] Z. Ahmad Dar,[3] F. Akbar,[3] D.A. Andrade,[4] G.D. Barr,[1] A. Bashyal,[5] A. Bercellie,[6] M. Betancourt,[7] A. Bodek,[6] A. Bravar,[8] H. Budd,[6] G. Caceres,[9] T. Cai,[6] M.F. Carneiro,[5,9,*] H. da Motta,[9] S.A. Dytman,[10] G.A. Díaz,[6,11] J. Felix,[4] L. Fields,[7] A. Filkins,[12] R. Fine,[6] A.M. Gago,[11] H. Gallagher,[2] A. Ghosh,[13,9] R. Gran,[14] D.A. Harris,[15,7] S. Henry,[6] S. Jena,[16] J. Kleykamp,[6] M. Kordosky,[12] D. Last,[17] T. Le,[2,18] A. Lozano,[9] X.-G. Lu,[1,†] E. Maher,[19] S. Manly,[6] W.A. Mann,[2] C. Mauger,[17] K.S. McFarland,[6] B. Messerly,[10] J. Miller,[13] J.G. Morfín,[7] D. Naples,[10] J.K. Nelson,[12] C. Nguyen,[20] A. Norrick,[12] A. Olivier,[6] V. Paolone,[10] G.N. Perdue,[7,6] M.A. Ramírez,[4] R.D. Ransome,[18] H. Ray,[20] D. Ruterbories,[6] H. Schellman,[5] J.T. Sobczyk,[21] C.J. Solano Salinas,[22] H. Su,[10] M. Sultana,[6] V.S. Syrotenko,[2] E. Valencia,[12,4] D. Wark,[1] A. Weber,[1] M.Wospakrik,[20] C. Wret,[6] B. Yaeggy,[13] and L. Zazueta[12]

(The MINERνA Collaboration)

[1] *Oxford University, Department of Physics, Oxford, OX1 3PJ United Kingdom*
[2] *Physics Department, Tufts University, Medford, Massachusetts 02155, USA*
[3] *AMU Campus, Aligarh, Uttar Pradesh 202001, India*
[4] *Campus León y Campus Guanajuato, Universidad de Guanajuato, Lascurain de Retana No. 5, Colonia Centro, Guanajuato 36000, Guanajuato México.*
[5] *Department of Physics, Oregon State University, Corvallis, Oregon 97331, USA*
[6] *University of Rochester, Rochester, New York 14627 USA*
[7] *Fermi National Accelerator Laboratory, Batavia, Illinois 60510, USA*
[8] *University of Geneva, 1211 Geneva 4, Switzerland*
[9] *Centro Brasileiro de Pesquisas Físicas, Rua Dr. Xavier Sigaud 150, Urca, Rio de Janeiro, Rio de Janeiro, 22290-180, Brazil*
[10] *Department of Physics and Astronomy, University of Pittsburgh, Pittsburgh, Pennsylvania 15260, USA*
[11] *Sección Física, Departamento de Ciencias, Pontificia Universidad Católica del Perú, Apartado 1761, Lima, Perú*
[12] *Department of Physics, College of William & Mary, Williamsburg, Virginia 23187, USA*
[13] *Departamento de Física, Universidad Técnica Federico Santa María, Avenida España 1680 Casilla 110-V, Valparaíso, Chile*
[14] *Department of Physics, University of Minnesota – Duluth, Duluth, Minnesota 55812, USA*
[15] *York University, Department of Physics and Astronomy, Toronto, Ontario, M3J 1P3 Canada*
[16] *Department of Physical Sciences, IISER Mohali, Knowledge City, SAS Nagar, Mohali - 140306, Punjab, India*
[17] *Department of Physics and Astronomy, University of Pennsylvania, Philadelphia, PA 19104*
[18] *Rutgers, The State University of New Jersey, Piscataway, New Jersey 08854, USA*
[19] *Massachusetts College of Liberal Arts, 375 Church Street, North Adams, MA 01247*
[20] *University of Florida, Department of Physics, Gainesville, FL 32611*
[21] *University of Wroclaw, plac Uniwersytecki 1, 50-137 Wrocaw, Poland*
[22] *Universidad Nacional de Ingeniería, Apartado 31139, Lima, Perú*

(Dated: February 17, 2020)

We study neutrino-induced charged-current π^0 production on carbon nuclei using events with fully imaged final-state proton-π^0 systems. Novel use of momentum variables enables measurements of the initial-state neutron momentum and of the final-state hadronic-system momentum balance relative to the leptonic system. Event distributions are presented for i) momenta of struck neutrons below and above the Fermi surface at 200 MeV/c, and ii) deviation of hadronic system momenta above and below the balance peak at 0 MeV/c. The measured shapes and absolute rates of these distributions show tensions with predictions from current neutrino generator models.

In high-statistics neutrino oscillation experiments [1–5], the measurement precision of the fundamental properties of neutrinos is becoming limited by knowledge of neutrino-nucleus interactions [6–8]. The dynamics arising from neutrinos scattering on bound nucleons is convolved with the primary neutrino-nucleon interaction. The nuclear medium introduces deviations from free-neutron scattering that are poorly known and are leading sources of systematic uncertainty for measurements of the $\mathcal{CP}$-violating phase [6, 7]. Limited knowledge of nuclear effects can lead to mis-reconstruction of the neutrino energy spectra and can compromise the evaluation of selection efficiencies for both signal and backgrounds [9].

Among the prominent interaction modes produced when studying neutrino flavor transformation are final states containing pions [8]. Although neutrino scattering measurements of pion topologies exist, they are either on light nuclei, such as hydrogen or deuterium [10–13], or else the analyses are restricted to kinematical vari-

This document was prepared by MINERvA collaboration using the resources of the Fermi National Accelerator Laboratory (Fermilab), a U.S. Department of Energy, Office of Science, HEP User Facility. Fermilab is managed by Fermi Research Alliance, LLC (FRA), acting under Contract No. DE-AC02-07CH11359.

ables with limited sensitivity to nuclear effects [14–19]. For future experiments such as DUNE [4] and Hyper-Kamiokande [5] to achieve their designed sensitivity it is imperative to assess the various nuclear effects involved in pion production.

In this Letter nuclear effects in carbon are evaluated by applying novel kinematic variables [20, 21] sensitive to such dynamics in neutrino-induced charged-current (CC) neutral-pion production. The primary bound-nucleon interaction producing the required hadronic final state, h, is

$$\nu_\mu + \mathrm{C} \to \mu^- + \underbrace{p + \pi^0}_{h} + \mathrm{X}, \tag{1}$$

where X is a final-state hadronic system that may contain nucleons and π^0s (no charged pions), which are induced by final-state interactions (FSI). FSI may lead to other neutrino-nucleon scattering processes, such as π^+ production on the proton, entering the final-state topology of interest. In addition to FSI, the Fermi-moving initial-state neutron may have nucleon-nucleon correlations that affect event kinematics. The nuclear medium therefore may give rise to an imbalance, $\delta\vec{p}$, between the incoming lepton's momentum and total momentum of the final state particles.

By taking advantage of this imbalance in final states containing $1\mu^- N\mathrm{p}M\pi^0$ $(N, M > 0)$ and any number of neutrons, the effects of the nuclear environment are probed using i) the reconstructed neutron momentum, p_n, of the initial state, and ii) the double-transverse momentum imbalance—the momentum imbalance of the final-state hadronic system transverse to the leptonic plane—δp_TT. The initial-state neutron momentum is calculated following the procedure described in [21, 22] according to

$$\begin{cases} \delta\vec{p}_\mathrm{T} = \vec{p}^{\,\mu}_\mathrm{T} + \vec{p}^{\,h}_\mathrm{T}, & (2) \\ \delta p_\mathrm{L} = \dfrac{1}{2}R - \dfrac{m^2_{\mathrm{A}'} + \delta\vec{p}^{\,2}_\mathrm{T}}{2R}, & (3) \\ R = m_\mathrm{A} + p^\mu_\mathrm{L} + p^h_\mathrm{L} - E^\mu - E^h, & (4) \\ p_\mathrm{n} = \left(\delta p^2_\mathrm{T} + \delta p^2_\mathrm{L}\right)^{1/2}. & (5) \end{cases}$$

Here, the subscripts T and L stand for transverse and longitudinal components with respect to the neutrino direction. The transverse, $\delta\vec{p}_\mathrm{T}$, and longitudinal, δp_L, components of the momentum imbalance are calculated using muon and hadron energies, E^μ and E^h, and momenta p^μ and p^h respectively. The longitudinal term includes the nuclear mass, $m_{\mathrm{A}^{(\prime)}}$, before and after the interaction by assuming the X is the remnant nucleus, A' only. We have $m_{\mathrm{A}'} = m_\mathrm{A} - m_\mathrm{n} - b$, where m_n is the neutron mass. For a carbon target, the excitation energy b is +28.7 MeV [21]. The variable p_n is highly useful as a probe of the nuclear medium because it separates the initial state from FSI.

The transverse component, $\delta\vec{p}_\mathrm{T}$, can be decomposed further to provide a complimentary means of probing nuclear effects [20, 23]. This is achieved using δp_TT – a kinematic imbalance of the final state hadronic system transverse to the neutrino direction, $\vec{d}_\nu$, and muon transverse momentum, $\vec{p}^{\,\mu}_\mathrm{T}$, plane [9]. The functional form is

$$\delta p_\mathrm{TT} = \frac{\vec{d}_\nu \times \vec{p}^{\,\mu}_\mathrm{T}}{\left|\vec{d}_\nu \times \vec{p}^{\,\mu}_\mathrm{T}\right|} \cdot \left(\vec{p}^{\,\mathrm{p}}_\mathrm{T} + \vec{p}^{\,\pi}_\mathrm{T}\right). \tag{6}$$

In the absence of nuclear effects the hadronic components balance, $\delta p_\mathrm{TT} = 0$, whereas for nuclei with A > 1, non-zero contributions arise from the nuclear medium.

In the present work, the signal is defined as charged-current ν_μ events on CH whose final state is $1\mu^- N\mathrm{p}M\pi^0$ $(N, M > 0)$ with any number of neutrons and no other particles exiting the nucleus. Kinematic constraints, resulting from detector acceptance and response, are placed on the final state satisfying

$$\begin{cases} 1.5 \le p_\mu \ (\mathrm{GeV}/c) \le 20.0, \ \theta_\mu < 25^\circ, & (7) \\ p_\mathrm{p} \ (\mathrm{MeV}/c) \ge 450, & (8) \end{cases}$$

where p_μ is the muon momentum, p_p is the leading proton momentum, and θ_μ is the muon polar angle with respect to the neutrino direction. The momenta of the leading proton and π^0 are used for computation. Measurements of p_n and δp_TT are presented and compared with various model predictions.

The analysis uses data obtained with the MINERνA detector exposed to the NuMI low energy neutrino beam ($\langle E_\nu \rangle$ = 3 GeV) with 3.33×10^{20} protons on target (POT). The total neutrino flux ($2.88 \times 10^{-8}/\mathrm{cm}^2/\mathrm{POT}$) is estimated according to Ref. [24]. Neutrino interactions inside a fiducial volume within MINERνA's active tracker with a mass of 5.3 tons are selected. Precise tracking is achieved inside this fiducial volume by an alternating arrangement of hexagonal plastic scintillator planes at 0° and ±60° to the vertical. Each plane consists of 127 triangular polystyrene (CH) strips up to 245 cm long, 1.7 cm in height and a width of 3.3 cm. The strips form a plane by alternating strips such that the cross sectional view is a regular trapezium. Located two meters downstream of MINERνA is the MINOS near detector—a magnetised muon spectrometer used to measure both the charge and momentum of muons. A detailed description of both detectors can be found in Refs [25, 26].

Neutrino events are simulated in the detector using GENIE 2.8.4 where the initial state is modeled as a relativistic global Fermi gas (RFG) [27]. GENIE describes CC Quasielastic (QE) processes following Ref. [28] with a dipole axial mass of 0.99 GeV [29]. The production of Δ and higher resonances used the Rein-Sehgal single pion model [30]. Non-resonant pion production and multi-pion resonance contributions are introduced with

a GENIE-specific model [31]. This background component is simulated up to a hadronic invariant mass range of $W < 1.7$ GeV [32–34]. All resonant baryons decay isotropically in their rest frame with the exception of the Δ^{++}. Following [15], the Δ^{++} angular isotropy is suppressed by 50% of that predicted by Rein-Seghal. Deep inelastic scattering (DIS) is incorporated into GENIE via the 2003 Bodek-Yang model [35] and hadronization is described by PYTHIA6 [36] and models based on Koba-Nielsen-Olesen scaling [37].

GENIE's default simulation is augmented to incorporate recent developments in both theory and experimental results. An additional two-particle-two-hole interaction mode outlined by the IFIC Valencia model [38, 39] is included; the relative strength has been scaled upwards in accord with the MINERνA inclusive scattering measurement [40]. Long-range correlations are also included in quasi-elastic interactions via the random phase approximation [38]. Finally a reduction of 53% in GENIE's non-resonant single pion prediction is applied in accord with recent analyses of deuterium bubble chamber data [33, 34]. GENIE applies an effective model of FSI based on Ref. [41].

The propagation of final state particles within the detector is simulated using GEANT4 9.4.2 [42]. Hadron test beam data provided by a scaled down version of MINERνA are used to constrain the GEANT4 simulation of protons and charged pions [25]. For both data and simulation the energy scale is calibrated using through-going muons. These procedures ensure that the energy deposited per plane agrees between data and simulation.

Signal-like events are selected by first requiring a single track originating from within MINERνA's tracker to match a negatively charged track identified by MINOS. This track must fulfill the kinematic constraints outlined in Eq. 7. The muon's starting position, or primary vertex, is assessed for the existence of any additional tracks. In instances where extra tracks exist the primary vertex is redetermined to account for the extra information provided by these tracks. All non-muon tracks are required to be proton-like by having their dE/dx profile compared to the simulated proton and $\pi^{\pm}$ ionization profiles using a likelihood ratio. Only proton-like tracks are retained and their profiles are used to determine their momentum. The leading proton must pass the phase-space requirement from Eq. 8.

Neutral pions are identified from their dominant decay signature, $\pi^0 \to \gamma\gamma$, by requiring exactly two electromagnetic showers. Their direction must be consistent with originating from the primary vertex or the event is rejected. The calorimetric energy and direction of both photons are combined to reconstruct the π^0's momentum. Any remaining charged pion background is reduced by requiring that no Michel electron-like signature exist in the candidate event. Full details of the selection can be found in [18] which used a much less restrictive event

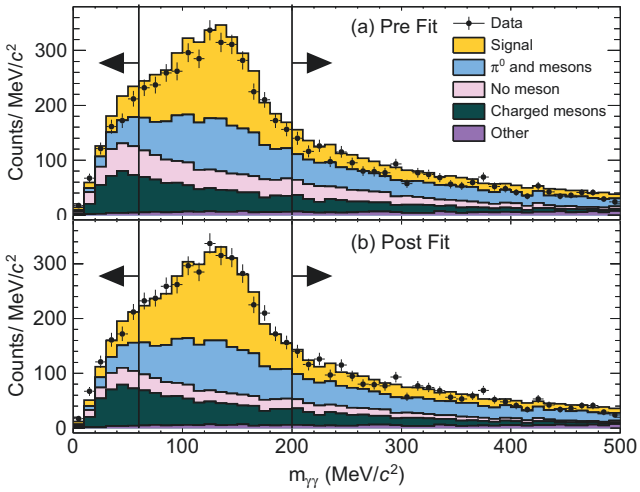

FIG. 1. Pre (a) and post (b) fit results for background constraints of the dominant topologies in the signal sample's photon invariant mass. The relative contributions from signal and backgrounds are displayed via stacked histograms. *Other* includes events failing to fulfil any of the above criteria, and $1\mu^- N\mathrm{p} M\pi^0$ $(N, M > 0)$ events which are out of acceptance.

phase space but required there be one and only one π^0 in the final state.

The signal purity is improved by reconstructing the invariant mass, $m_{\gamma\gamma}$, of the two photons using

$$m_{\gamma\gamma} = \left[E_1 E_2 \left(1 - \cos\theta_{12}\right)\right]^{1/2}. \tag{9}$$

Here E_1 and E_2 are the high and low energy photons respectively, whose opening angle is θ_{12}. Signal events are required to be within $60 \leq m_{\gamma\gamma}$ (MeV/c) ≤ 200 resulting in a 51.4% purity and 5.7% efficiency in this region as seen in Fig. 1. The dominant background topologies are (in decreasing order of importance) π^0s with charged mesons, only charged mesons, and zero meson events.

A data-driven approach is used to constrain the MC background components with a set of three sidebands. One sideband utilized events below and above the $m_{\gamma\gamma}$ range allowed to the selected sample. A second sideband used events that satisfied the signal definition except for the quality requirements for proton tracks. The third sideband used events that satisfied the signal definition but were accompanied by a Michel electron tag (indicating presence of a π^+ track). Events were accepted in the latter sideband sample if they did not possess a non-muon track; if a track was present, it was required to be proton-like. The normalizations of these three backgrounds are tuned to describe the data in the sidebands. The result can be seen in Fig. 2 for the reconstructed p_{n} and δp_{TT} before background subtraction.

The reconstructed proton momentum resolution is improved by selecting elastically scattered and contained protons via an additional criterion that requires a large $\mathrm{d}E/\mathrm{d}x$ near the track end-points [43]. As a result this re-

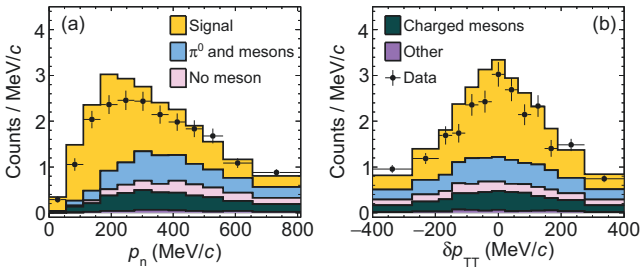

FIG. 2. Reconstructed p_n (a) and δp_{TT} (b) data before background subtraction is compared to tuned GENIE +GEANT4 simulation.

moves ill-determined momentum estimated events whose highest-momentum protons either undergo inelastic scattering or are not contained in the tracker. This leads to a 57% increase in p_p resolution albeit at the cost of a 50% reduction in statistics.

The π^0 momentum reconstruction is improved via an optimization technique that incorporates MINERνA's precise tracking in its determination. Given the relationship between the known π^0 invariant mass, photon energies and angle in Eq. 9, the measured energies, E_i, are recalculated by minimizing

$$\chi^2 = \left[\frac{m_\pi^2 - E_1 E_2 (1-\cos\theta_{12})}{\sigma_{m_\pi^2}}\right]^2 + \sum_{i=1}^{2}\left[\frac{E_i - E_i'}{\sigma(E_i)}\right]^2. \quad (10)$$

The latter term acts as a penalty for each photon and ensures that the fitted energies are within expectation of their calorimetrically measured, E_i', values. Note that $\sigma_{m_\pi^2}$ is used as an optimisation parameter whose value is chosen such that 99% of the fits successfully converge. Both $\sigma_{m_\pi^2}$ and each photon's energy-dependent resolution, $\sigma(E_i)$, are determined from simulation. A full description can be found in Ref. [23]. This improves the π^0 momentum resolution by 10%.

Flux integrated cross sections are produced by subtracting the constrained backgrounds from each observable. D'Agostini unfolding [44] is then performed with 4 iterations. The unfolding procedure is validated by reproducing pseudodata that is produced by extreme variations of the cross section models. The efficiency correction is then made before being normalized by the product of the flux and number of target nucleons (3.12×10^{30}). Systematic uncertainties are evaluated for all observables following Ref. [18]. For example, p_n whose statistical uncertainty spans 10–34% has systematic uncertainties arising from detector (2–8%), flux (3–8%), and GENIE cross section models (5-28%). The total uncertainty for p_n at few MeV/c is approximately 22% increasing to 46% at 800 MeV/c. (See the Supplement 1 [45] and 2 [46] for full description of cross-section uncertainties.)

The measured differential cross section in p_n is shown in Fig. 3. Its prominent feature is a peak at around 0.2 GeV/c. This is qualitatively captured by the NuWro (19.02) [47] RFG model [Fig. 3(a)]. In this Fermi gas model, all nucleons lie below the Fermi surface; without FSI, the p_n calculated from the exclusive proton-π^0 production represents neutron Fermi motion that shows a cut-off at 220 MeV/c (for illustration cf. Fig. 5 of Ref. [48]). The non-exclusive part of the signal [$1\mu^- N\mathrm{p} M\pi^0$ ($N, M > 0$), with $N + M > 2$, such as multi-π^0 production], characterized by large momentum imbalance, gives rise to p_n larger than the Fermi motion, and hence the long tail in the no-FSI RFG prediction. With FSI, kinematic distortion migrates events away from the Fermi motion peak; pion absorption and charge exchange following multi-π contributions and wrong-sign (Δ^{++}) production, respectively, also add to the tail region. The resulting tail is similar in the RFG and the NuWro/GENIE (2.12.10) local Fermi-gas (LFG) predictions, all describing data within about 1-σ. However, the data, in contrast to conventional implementations of RFG and LFG that are standard in current event generators, exhibit a distinctly muted distribution be-

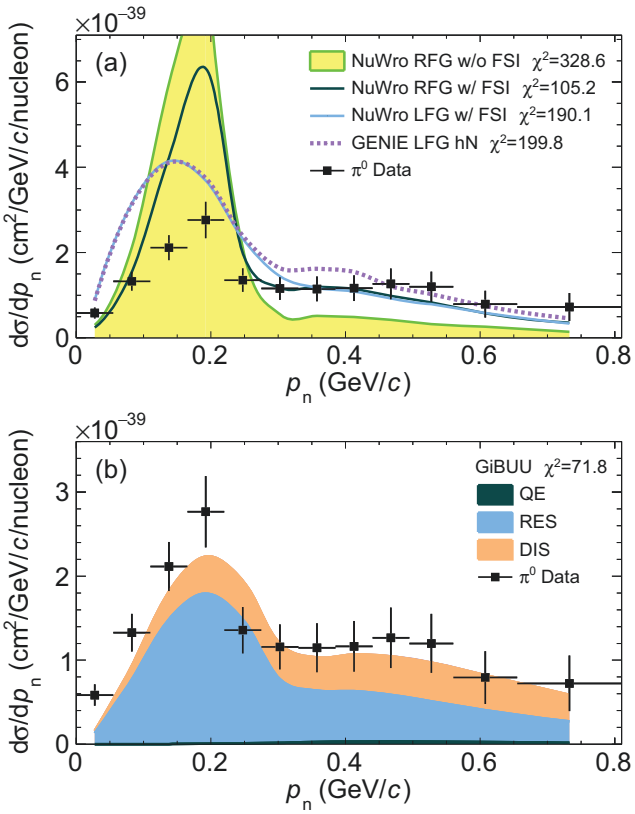

FIG. 3. Differential cross section in p_n compared to NuWro 19.02 and GENIE 2.12.10 (with the hN FSI) with various initial-state models (a), as well as to GiBUU 2019 predictions (b). The prediction of a NuWro RFG without FSI whose maximum is 8.9×10^{-42} cm^2/MeV/c/nucleon is also shown. Error bars on the data include both statistical and systematic uncertainties.

low 300 MeV/c—devoid of the sharp falloff in momentum that is conventionally associated with the top of the Fermi sea. Furthermore, the LFG peak locates at around 0.15 GeV/c, 25% off compared to data. In recent measurements of $p_{\rm n}$ in pionless production [49, 50] the Spectral Function (SF) approach best describes the data. However at present, while SF calculations for pion production exist [51, 52], they are not yet implemented in generators.

Comparison is also made to GiBUU (2019) [53, 54] predictions in Fig. 3(b). While it also describes the tail region, GiBUU underpredicts the Fermi motion peak and is skewed left with respect to the data. Nevertheless, it has the correct peak location and overall better describes the data, giving a smaller χ^2 compared to that of other generators. In GiBUU, the initial state is also modeled as LFG but in a nuclear potential [55]; the improvement relative to NuWro and GENIE LFG might indicate the importance of using a realistic nuclear potential in pion production. Yet, other model features that decrease or enhance the exclusive proton-π^0 production will have as large an effect on the agreement as the initial state. From the decomposition of the interaction mode, it can be seen that besides the dominant resonance production (RES), the DIS has a sizeable contribution that tends to be uniform in $p_{\rm n}$. This is also the prediction of GENIE and NuWro. Quasielastic events wherein proton FSI initiates π^0 production give a negligible contribution.

The $\delta p_{\rm TT}$ differential cross section in Fig. 4(a) shows clear disagreement between data and NuWro/GENIE predictions. Some improvement with description of the peak region in the data is obtained with utilization of LFG in the models. Here, the data distribution peaks at zero momentum imbalance as do the RFG predictions, however the data approaches either side of the peak with slope changes that are opposite to those of the predicted distributions. Fig. 4(b) shows that GiBUU provides a better description, however this model underpredicts the event rate into bins in the vicinity of the peak.

For initial-state neutrons with negligible Fermi motion, in the case of no FSI, the proton-π^0 momenta from exclusive reactions will be balanced with respect to the lepton scattering plane, yielding $\delta p_{\rm TT}= 0$. Fermi motion and non-exclusive contributions then introduce event-by-event imbalance equally on both sides of the plane. Due to possible polarization effects associated with the Δ production, the final-state π^0 could prefer one side of the scattering plane, as observed in the previous measurement [18] (see also Ref. [56] for discussion). As a result, one expects a positive-negative asymmetry in $\delta p_{\rm TT}$ as the proton and π^0 final states experience different momentum exchange inside the nucleus during FSI. In this measurement, the measured cross-section asymmetries of each positive-negative $\delta p_{\rm TT}$-bin pairs [defined as $(\mathrm{d}\sigma_+ - \mathrm{d}\sigma_-)/(\mathrm{d}\sigma_+ + \mathrm{d}\sigma_-)$] are about 0.2 at 1-$\sigma$ level, whereas negligible asymmetry is predicted by the generators where no polarization effect is modeled.

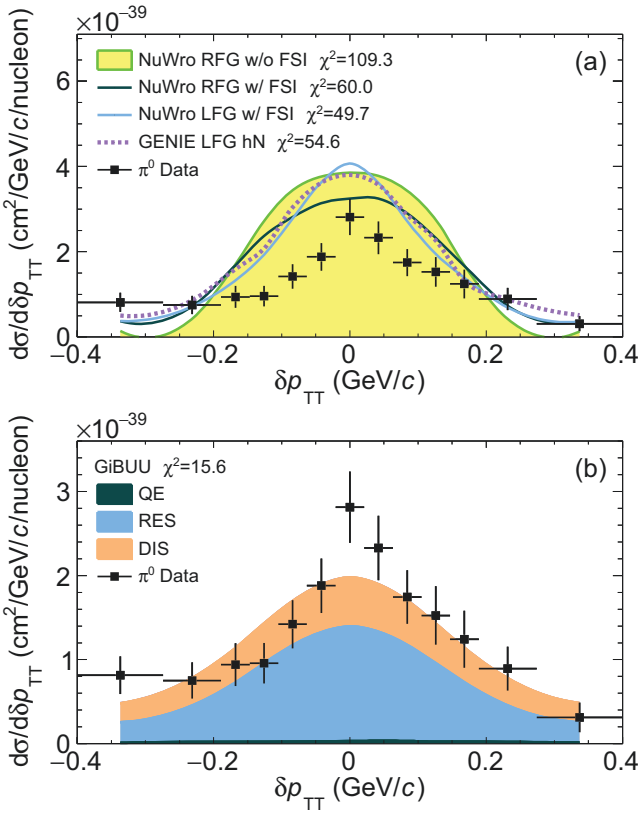

FIG. 4. Differential cross section in $\delta p_{\rm TT}$ compared to NuWro 19.02, GENIE 2.12.10 (a), and GiBUU 2019 (b) predictions.

In summary, this Letter presents the first measurement of neutrino proton-π^0 production cross section as functions of the initial-state neutron momentum, $p_{\rm n}$, and of the hadronic system momentum imbalance transverse to the leptonic plane, $\delta p_{\rm TT}$. Similar analysis methods were used in previous measurements of CC pionless production [49, 50] where the initial state was successfully described using Spectral Functions, an approach that has yet to be tried with CC pion production. In the present measurement, RFG and LFG models describe within 1-σ the large momentum imbalance region, $p_{\rm n}>$ 300 MeV/c, that collectively come from short-range correlations, FSI distortions, non-exclusive contributions, and wrong-sign (Δ^{++}) production. The exclusive proton-π^0 production cross section on neutrons in nuclei with $p_{\rm n}<$ 220 MeV/c, however, is mismodeled by generators using various Fermi gases. Further quantification of the final-state hadronic momentum configuration is made by $\delta p_{\rm TT}$ which shows a mild asymmetry that could come from particle-dependent FSI following polarization effects associated with the Δ production.

In the future, nuclear effects with initial-state proton momenta could be examined using proton-$\pi^{\pm}$ produc-

tion in CC ν_μ and $\overline{\nu}_\mu$ nucleus scattering [21]. Measurements of proton-π^0 systems as reported here could be performed in liquid argon TPC experiments such as ICARUS [57], MicroBooNE [58, 59], and SBND [57], providing clarifications of neutrino-argon interactions that are needed by the DUNE neutrino oscillation program. MINERνAs medium-energy exposures allow new investigations at higher neutrino energies and with larger event samples [60]. Thus, further illumination of the physics that underwrites $p_{\rm n}$ and $\delta p_{\rm TT}$ distributions in CC pion production may be anticipated.

This document was prepared by members of the MINERνA Collaboration using the resources of the Fermi National Accelerator Laboratory (Fermilab), a U.S. Department of Energy, Office of Science, HEP User Facility. Fermilab is managed by Fermi Research Alliance, LLC (FRA), acting under Contract No. DE-AC02-07CH11359. These resources included support for the MINERνA construction project, and support for construction also was granted by the United States National Science Foundation under Award No. PHY-0619727 and by the University of Rochester. Support for participating scientists was provided by NSF and DOE (USA); by CAPES and CNPq (Brazil); by CoNaCyT (Mexico); by Proyecto Basal FB 0821, CONICYT PIA ACT1413, Fondecyt 3170845 and 11130133 (Chile); by CONCYTEC (Consejo Nacional de Ciencia, Tecnologa e Innovacin Tecnolgica), DGI-PUCP (Direccin de Gestin de la Investigacin - Pontificia Universidad Catlica del Peru), and VRI-UNI (Vice-Rectorate for Research of National University of Engineering) (Peru); and by the Latin American Center for Physics (CLAF); NCN Opus Grant No. 2016/21/B/ST2/01092 (Poland); by Magdalen College Oxford and Science and Technology Facilities Council (UK). We thank the MINOS Collaboration for use of its near detector data. Finally, we thank the staff of Fermilab for support of the beam line, the detector, and computing infrastructure.

* Now at Brookhaven National Laboratory
† Corresponding author:Xianguo.Lu@physics.ox.ac.uk

[1] K. Abe *et al.* (T2K), Nucl. Instrum. Meth. **A659**, 106 (2011), arXiv:1106.1238 [physics.ins-det].
[2] D. S. Ayres *et al.* (NOvA), (2007), 10.2172/935497.
[3] K. Abe *et al.*, (2011), arXiv:1109.3262 [hep-ex].
[4] R. Acciarri *et al.* (DUNE), (2015), arXiv:1512.06148 [physics.ins-det].
[5] K. Abe *et al.* (Hyper-Kamiokande Proto-Collaboration), PTEP **2015**, 053C02 (2015), arXiv:1502.05199 [hep-ex].
[6] P. Adamson *et al.* (NOvA), Phys. Rev. Lett. **118**, 151802 (2017), arXiv:1701.05891 [hep-ex].
[7] K. Abe *et al.* (T2K), Phys. Rev. **D96**, 092006 (2017), [Erratum: Phys. Rev.D98,no.1,019902(2018)], arXiv:1707.01048 [hep-ex].
[8] L. Alvarez-Ruso *et al.*, Prog. Part. Nucl. Phys. **100**, 1 (2018), arXiv:1706.03621 [hep-ph].
[9] D. Coplowe, X.-G. Lu, and G. Barr (T2K), *Proceedings, 27th International Conference on Neutrino Physics and Astrophysics (Neutrino 2016): London, United Kingdom, July 4-9, 2016*, J. Phys. Conf. Ser. **888**, 012173 (2017), arXiv:1610.06244 [hep-ex].
[10] J. Campbell, G. Charlton, Y. Cho, M. Derrick, R. Engelmann, J. Fetkovich, L. Hymah, K. Jaeger, D. Jankowski, A. Mann, U. Mehtani, B. Musgrave, P. Schreiner, T. Wangler, J. Whitmore, and H. Yuta, Phys. Rev. Lett. **30**, 335 (1973).
[11] J. Bell *et al.*, Phys. Rev. Lett. **41**, 1008 (1978).
[12] S. J. Barish *et al.*, Phys. Rev. **D19**, 2521 (1979).
[13] G. M. Radecky *et al.*, Phys. Rev. **D25**, 1161 (1982), [Erratum: Phys. Rev.D26,3297(1982)].
[14] K. Abe *et al.* (T2K), Phys. Rev. **D95**, 012010 (2017), arXiv:1605.07964 [hep-ex].
[15] B. Eberly *et al.* (MINERvA), Phys. Rev. **D92**, 092008 (2015), arXiv:1406.6415 [hep-ex].
[16] T. Le *et al.* (MINERvA), Phys. Lett. **B749**, 130 (2015), arXiv:1503.02107 [hep-ex].
[17] C. L. McGivern *et al.* (MINERvA), Phys. Rev. **D94**, 052005 (2016), arXiv:1606.07127 [hep-ex].
[18] O. Altinok *et al.* (MINERvA), Phys. Rev. **D96**, 072003 (2017), arXiv:1708.03723 [hep-ex].
[19] T. Le *et al.* (MINERvA), Phys. Rev. **D100**, 052008 (2019), arXiv:1906.08300 [hep-ex].
[20] X.-G. Lu, D. Coplowe, R. Shah, G. Barr, D. Wark, and A. Weber, Phys. Rev. **D92**, 051302 (2015), arXiv:1507.00967 [hep-ex].
[21] X.-G. Lu and J. T. Sobczyk, Phys. Rev. **C99**, 055504 (2019), arXiv:1901.06411 [hep-ph].
[22] A. P. Furmanski and J. T. Sobczyk, Phys. Rev. **C95**, 065501 (2017), arXiv:1609.03530 [hep-ex].
[23] D. Coplowe, *Probing Nuclear Effects in Neutrino Induced Pion Production*, Ph.D. thesis, University of Oxford (2018).
[24] L. Aliaga *et al.* (MINERvA), Phys. Rev. **D94**, 092005 (2016), [Addendum: Phys. Rev.D95,no.3,039903(2017)], arXiv:1607.00704 [hep-ex].
[25] L. Aliaga *et al.* (MINERvA), Nucl. Instrum. Meth. **A743**, 130 (2014), arXiv:1305.5199 [physics.ins-det].
[26] D. G. Michael *et al.* (MINOS), Nucl. Instrum. Meth. **A596**, 190 (2008), arXiv:0805.3170 [physics.ins-det].
[27] A. Bodek and J. L. Ritchie, Phys. Rev. **D23**, 1070 (1981).
[28] C. H. Llewellyn Smith, *Gauge Theories and Neutrino Physics, Jacob, 1978:0175*, Phys. Rept. **3**, 261 (1972).
[29] R. Bradford, A. Bodek, H. S. Budd, and J. Arrington, *NuInt05, proceedings of the 4th International Workshop on Neutrino-Nucleus Interactions in the Few-GeV Region, Okayama, Japan, 26-29 September 2005*, Nucl. Phys. Proc. Suppl. **159**, 127 (2006), [,127(2006)],

arXiv:hep-ex/0602017 [hep-ex].
[30] D. Rein and L. M. Sehgal, Annals Phys. **133**, 79 (1981).
[31] A. Bodek, I. Park, and U.-k. Yang, *Proceedings, 3rd International Workshop on Neutrino-nucleus interactions in the few GeV region (NUINT 04): Assergi, Italy, March 17-21, 2004*, Nucl. Phys. Proc. Suppl. **139**, 113 (2005), [,113(2004)], arXiv:hep-ph/0411202 [hep-ph].
[32] H. Gallagher, Nuclear Physics B - Proceedings Supplements **159**, 229 (2006), proceedings of the 4th International Workshop on Neutrino-Nucleus Interactions in the Few-GeV Region.
[33] C. Wilkinson, P. Rodrigues, S. Cartwright, L. Thompson, and K. McFarland, Phys. Rev. **D90**, 112017 (2014), arXiv:1411.4482 [hep-ex].
[34] P. Rodrigues, C. Wilkinson, and K. McFarland, Eur. Phys. J. **C76**, 474 (2016), arXiv:1601.01888 [hep-ex].
[35] A. Bodek and U. K. Yang, *Neutrino factories. Proceedings, 4th International Workshop, NuFact'02, London, UK, July 1-6, 2002*, J. Phys. **G29**, 1899 (2003), arXiv:hep-ex/0210024 [hep-ex].
[36] T. Sjostrand, S. Mrenna, and P. Z. Skands, JHEP **05**, 026 (2006), arXiv:hep-ph/0603175 [hep-ph].
[37] Z. Koba, H. B. Nielsen, and P. Olesen, Nucl. Phys. **B40**, 317 (1972).
[38] J. Nieves, J. E. Amaro, and M. Valverde, Phys. Rev. **C70**, 055503 (2004), [Erratum: Phys. Rev.C72,019902(2005)], arXiv:nucl-th/0408005 [nucl-th].
[39] R. Gran, J. Nieves, F. Sanchez, and M. J. Vicente Vacas, Phys. Rev. **D88**, 113007 (2013), arXiv:1307.8105 [hep-ph].
[40] P. A. Rodrigues *et al.* (MINERvA), Phys. Rev. Lett. **116**, 071802 (2016), [Addendum: Phys. Rev. Lett.121,no.20,209902(2018)], arXiv:1511.05944 [hep-ex].
[41] S. A. Dytman and A. S. Meyer, AIP Conference Proceedings **1405**, 213 (2011), https://aip.scitation.org/doi/pdf/10.1063/1.3661588.
[42] S. Agostinelli *et al.* (GEANT4), Nucl. Instrum. Meth. **A506**, 250 (2003).
[43] X.-G. Lu and M. Betancourt (MINERvA), *Proceedings, 27th International Conference on Neutrino Physics and Astrophysics (Neutrino 2016): London, United Kingdom, July 4-9, 2016*, J. Phys. Conf. Ser. **888**, 012120 (2017), arXiv:1608.04655 [hep-ex].
[44] G. D'Agostini, Nucl. Instrum. Meth. **A362**, 487 (1995).
[45] Supplemental Material 1 ().
[46] Supplemental Material 2 ().
[47] T. Golan, C. Juszczak, and J. T. Sobczyk, Phys. Rev. **C86**, 015505 (2012), arXiv:1202.4197 [nucl-th].
[48] L. Pickering, *Proceedings, 10th International Workshop on Neutrino-Nucleus Interactions in the Few GeV Region (NuInt15): Osaka, Japan, November 16-21, 2015*, JPS Conf. Proc. **12**, 010032 (2016), arXiv:1602.06730 [hep-ex].
[49] X.-G. Lu *et al.* (MINERvA), Phys. Rev. Lett. **121**, 022504 (2018), arXiv:1805.05486 [hep-ex].
[50] K. Abe *et al.* (T2K), Phys. Rev. **D98**, 032003 (2018), arXiv:1802.05078 [hep-ex].
[51] H. Nakamura, M. Sakuda, T. Nasu, and O. Benhar, Phys. Rev. **C76**, 065208 (2007), arXiv:0705.3884 [hep-ph].
[52] H. Nakamura, T. Nasu, M. Sakuda, and O. Benhar, *Neutrino factories, superbeams and betabeams. Proceedings, 9th International Workshop, NuFact07, Okayama, Japan, August 6-11, 2007*, AIP Conf. Proc. **981**, 234 (2008).
[53] O. Buss, T. Gaitanos, K. Gallmeister, H. van Hees, M. Kaskulov, O. Lalakulich, A. B. Larionov, T. Leitner, J. Weil, and U. Mosel, Phys. Rept. **512**, 1 (2012), arXiv:1106.1344 [hep-ph].
[54] K. Gallmeister, U. Mosel, and J. Weil, Phys. Rev. **C94**, 035502 (2016), arXiv:1605.09391 [nucl-th].
[55] U. Mosel, J. Phys. **G46**, 113001 (2019), arXiv:1904.11506 [hep-ex].
[56] T. Cai, X.-G. Lu, and D. Ruterbories, Phys. Rev. **D100**, 073010 (2019), arXiv:1907.11212 [hep-ex].
[57] M. Antonello *et al.* (MicroBooNE, LAr1-ND, ICARUS-WA104), (2015), arXiv:1503.01520 [physics.ins-det].
[58] MicroBooNE, MICROBOONE-NOTE-1056-PUB (2018), 10.2172/15
[59] C. Adams *et al.* (MicroBooNE), Phys. Rev. **D99**, 091102 (2019), arXiv:1811.02700 [hep-ex].
[60] E. Valencia *et al.* (MINERvA), (2019), arXiv:1906.00111 [hep-ex].